Water Research 254 (2024) 121386

Contents lists available at ScienceDirect

Water Research

journal homepage: www.elsevier.com/locate/watres

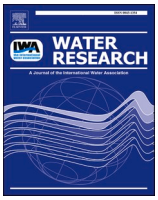

Dielectric barrier discharge plasma promotes disinfection-residual-bacteria inactivation via electric field and reactive species

Ruoyu Deng [a,b], Qiang He [a,b], Dongxu Yang [a,b], Mengli Chen [a,b], Yi Chen [a,b,*]

[a] Key Laboratory of the Three Gorges Reservoir Region's Eco-Environment, Ministry of Education, Chongqing University, Chongqing, 400045, China
[b] College of Environment and Ecology, Chongqing University, Chongqing, 400045, China

ARTICLE INFO

Keywords:
Bacteria inactivation
Dielectric barrier discharge plasma
Disinfection-residual-bacteria
Electric field
Basic discharge unit model

ABSTRACT

Traditional disinfection processes face significant challenges such as health and ecological risks associated with disinfection-residual-bacteria due to their single mechanism of action. Development of new disinfection processes with composite mechanisms is therefore urgently needed. In this study, we employed liquid ground-electrode dielectric barrier discharge (lgDBD) to achieve synergistic sterilization through electric field electroporation and reactive species oxidation. At a voltage of 12 kV, *Pseudomonas fluorescens* (ultraviolet and ozone-resistant) and *Bacillus subtilis* (chlorine-resistant) were completely inactivated within 8 and 6 min, respectively, surpassing a 7.0-log reduction. The lgDBD process showed good disinfection performance across a wide range of pH values and different practical water samples. Staining experiments suggest that cellular membrane damage contributes to this inactivation. In addition, we used a two-dimensional parallel streamer solver with kinetics code to fashion a representative model of the basic discharge unit, and discovered the presence of a persistent electric field during the discharge process with a peak value of 2.86×10^6 V/m. Plasma discharge generates excited state species such as $O(^1D)$ and $N_2(C^3\Pi_u)$, and further forms reactive oxygen and nitrogen species at the gas-liquid interface. The physical process, which is driven by electric field-induced cell membrane electroporation, synergizes with the bactericidal effects of reactive oxygen and nitrogen species to provide effective disinfection. Adopting the lgDBD process enhances sterilization efficiency and adaptability, underscoring its potential to revolutionize physicochemical synergistic disinfection practices.

1. Introduction

Water treatment necessitates rigorous disinfection in order to counteract the significant threats posed by bacteria and other pathogenic microorganisms to water biosecurity (Tang et al., 2023; Zhang et al., 2021). Prominent methods such as chlorine (Pfaller et al., 2021; Wang et al., 2023a), ultraviolet (UV) (Wang et al., 2022b; Zhang et al., 2019), and ozone disinfection (Jung et al., 2008; Pak et al., 2016) are favored due to their economic and versatile application. However, each of these methods is limited by its single mechanism of action, which can leave some microorganisms less affected (Cao et al., 2023; Waso et al., 2020). Such disinfection processes exert a significant selective effect on bacteria in the water. These residual bacteria, referred to as disinfection-residual-bacteria (DRB), often possess one or multiple forms of disinfection resistance. For example, *Bacillus subtilis* has been found to have resistance to chlorine disinfection (Luo et al., 2021), and *Pseudomonas fluorescens* has shown resistance to ultraviolet and ozone (Wang et al., 2021a). The relative abundance of these organisms significantly increases after treatment with these corresponding disinfection methods, posing health, procedural, and ecological risks (Tang et al., 2023; Wang et al., 2021a). The existence of DRB only exacerbates the challenge involved with tackling waterborne microbial threats.

Developing new disinfection processes with composite disinfection mechanisms can effectively address the resistance of DRB to disinfectants (Liu et al., 2022a; Sharma et al., 2015; Wu et al., 2023). Ozone, with its remarkable oxidative potential, is widely used in water disinfection (Morrison et al., 2022). Its primary mode of action involves interacting with unsaturated lipids in bacterial cell membranes and peptidoglycans in cell walls, leading to bacterial cell lysis (Hogard et al., 2023). However, the ozone resistance of microorganisms, coupled with the short lifespan of ozone, often hamper its efficacy (Zhou et al., 2020). In traditional procedures, ozone production and application are segregated into two separate reactors: ozone generated from plasma discharges is transported via pipelines and then infused into the water

* Corresponding author at: 174 Shazhengjie Street, Shapingba District, Chongqing 400045, China.
E-mail address: chenyi8574@cqu.edu.cn (Y. Chen).

https://doi.org/10.1016/j.watres.2024.121386
Received 12 December 2023; Received in revised form 2 February 2024; Accepted 25 February 2024
Available online 1 March 2024

(El-Athman et al., 2021). This separation reduces the oxidative strength of ozone and misses out on the synergistic advantages of associated phenomena during plasma discharge, such as excited states species, UV radiation, and electric fields (Deng et al., 2023). Therefore, integrating the processes of ozone generation and application into a single reactor can enrich the disinfection mechanisms and significantly enhance sterilization efficiency.

Numerous researchers including the author's team are delving into an innovative water disinfection method that incorporates composite disinfection mechanisms: liquid ground-electrode dielectric barrier discharge (lgDBD) plasma process (Guo et al., 2019; Wu et al., 2020). In this process, water as the ground-electrode undergoes in-situ contact with the discharge plasma in the lgDBD reactor. This produces not only ozone but also a plethora of other agents, such as short-lived reactive species, excited states species, and UV light, each potential contributors to bacterial deactivation (Aka et al., 2022; Patinglag et al., 2021; Patinglag et al., 2019; Van de Moortel et al. 2017; Wang et al., 2021b; Wang et al., 2018). The effects of common reactive oxygen species (ROS) such as ozone, H_2O_2, and ·OH have been extensively studied (Nau-Hix et al., 2021; Pancheshnyi et al., 2005; Shen et al., 2023; Stratton et al., 2017; Wang et al., 2023a; Wang et al., 2023b; Yu et al., 2012; Zhou et al., 2020). However, the role of physical processes such as electric field energization in the sterilization process remains unclear. This is primarily because the time scale of each basic discharge unit is on the order of nanoseconds (Yin et al., 2023). Moreover, at the microscopic level, the discharge process generates a response electric field that is stronger than the original electric field. The presence of this response electric field causes dramatic changes in the electric field of the discharge area over extremely short time scales that are beyond the reach of traditional detection methods (Zhu et al., 2017). Therefore, current research predominantly focuses on the response of the aqueous phase in plasma discharge (Deng et al., 2021; Guo et al., 2023; Singh et al., 2019b; Singh et al., 2020), while often neglecting aspects directly related to the discharge itself, such as electric field strength and free electron concentration. Electroporation is a physical sterilization method that is applied to treat water (Huo et al., 2022). It damages the membrane structure of bacteria by using a strong electric field and has the advantages of low energy consumption and a total lack of disinfection by-products (Huo et al., 2023a; Huo et al., 2023b). However, electroporation requires an electric field of more than 10^6 V/m (Wang et al., 2022a). Therefore, it is necessary to determine whether lgDBD can generate a sufficiently strong electric field for sterilization and to measure the contribution of the electric field effect in the sterilization process.

The multiple mechanisms of lgDBD, based on both physical and chemical processes, offer intriguing insights when explored in the context of disinfection. In this study, *Bacillus subtilis* (chlorine-resistant) and *Pseudomonas fluorescens* (resistant to ultraviolet and ozone) were selected as models for Gram-positive and Gram-negative bacteria, respectively, and their inactivation efficiency in lgDBD was investigated (Wang et al., 2021a). The effects of voltage and discharge gases on disinfection efficacy were examined. Damage to the bacterial cell membrane was analysed using flow cytometry and confocal microscopy. Furthermore, using the two-dimensional (2D) parallel streamer solver with kinetics (PASSKEy) code, we constructed a model for the basic discharge unit. Combined with various assessments of the reactive species, the role, and bactericidal contributions of the electric field to disinfection, ROS and reactive nitrogen species (RNS) were investigated, allowing us finally to report a novel synergistic bactericidal mechanism.

2. Materials and methods

2.1. Experimental setup

Chemicals, reagents, and microbial cultures are described in the Supporting Information (Text S1). As depicted in Fig. S1, the lgDBD sterilization apparatus consisted of a high-voltage power supply (CTP-2000 K, Coronalab), a regulator (Coronalab), a lgDBD reactor, and an oscilloscope (DS1000E, Rigol). The discharge surface of the lgDBD reactor had a diameter of 50 mm, with a discharge gap height of 6 mm. The oscilloscope measured the voltage-current curve through the output voltage and current detection interface built into the power supply. The output voltage was measured after being reduced by a 1:1000 scale, where the sampling resistor for the output current was 50 Ω, and the sampling capacitor was 0.47 μF.

Bacterial inactivation experiments were conducted in the lgDBD reactor. Initially, the experimental bacterial strains were cultivated to the logarithmic growth phase. *Pseudomonas fluorescens* and *Bacillus subtilis* were both cultured using nutrient broth medium, with *Pseudomonas fluorescens* incubated at 25 °C for 36 h and *Bacillus subtilis* at 30 °C for 48 h. After the bacterial cultures reached the desired growth phase, they were centrifuged (3000 rpm, 5 min) using a high-speed centrifuge and resuspended in phosphate-buffered saline (PBS) to avoid the interference of continued oxidative capacity in water on subsequent analysis. The bacterial suspension was then diluted with PBS to achieve a concentration of approximately 10^7 CFU/mL. Next, 100 mL of the bacterial suspension was placed into a water storage bottle, and 100 mL/min peristaltic pump was used to circulate the bacterial suspension between the water storage bottle and the lgDBD reactor. The output voltage of the high-voltage power supply was set to range between 9 kV and 12 kV, with a frequency of 9.2 kHz. After the reaction, the samples were centrifuged again and resuspended in PBS.

For ozone treatment experiments and UV treatment experiments, additional details are provided in the Supporting Information (Text S2). The calculation methods for discharge power, pseudo-first-order inactivation rate constants, energy efficiencies ($G_{6\text{-log}}$), and electrical energy per order (E_{EO}) are further described in the Supporting Information (Text S3).

2.2. Analytical methods

Bacterial liquid concentrations were enumerated using the spread plate method. For scanning electron microscopy (SEM) analysis, bacterial samples were fixed with 2.5 % glutaraldehyde for 24 h, followed by fixation with 1 % osmium tetroxide solution for 2 h. After ethanol gradient dehydration, the samples were critically dried and imaged using a German ZEISS Sigma 300 scanning electron microscope to visualize the morphologies of *Pseudomonas fluorescens* and *Bacillus subtilis*.

For co-localization microscopy and flow cytometry analysis, dual-staining with SYTO™ 9 and propidium iodide (PI) was performed. The bacterial samples were incubated at room temperature in the dark for 15 min, followed by testing using a confocal microscope (TCS SP8 DIVE, Leica, Germany) and a flow cytometer (BD Fortessa).

Optical emission spectra (OES) were obtained using a spectrometer (AvaSpec-ULS3648-USB2-UA-25). Electron paramagnetic resonance (EPR) spectra were acquired using 5,5-Dimethyl-1-pyrroline N-oxide (DMPO) and 2,2,6,6-tetramethylpiperidine (TEMP) as trapping agents on an EPR200-Plus instrument (Chinainstru & Quantumtech, Hefei).

The concentrations of H_2O_2, dissolved O_3, and NO_3^- in the water were determined using the titanium oxalate method, sodium indigo disulfonate colorimetric method, and ultraviolet spectrophotometry, respectively, with detailed descriptions available in the Supporting Information (Text S4).

2.3. Basic discharge unit modeling

A 2D model of the lgDBD reactor was created using the PASSKEy code. The numerical methods and validation of the PASSKEy code against benchmark cases have been extensively described in previous studies (Mao et al., 2022; Zhu et al., 2017). Here, the computational domain was set at 50 mm × 50 mm, and a prescribed input voltage of 12 kV was applied. The gas composition used was air. The geometric

structure is illustrated in Fig. 4a. Four types of materials were set up in the model: plasma, ground electrode, driven electrode, and neutral gas. For the plasma, the dynamic simulation scheme proposed by Pancheshnyi (Pancheshnyi et al., 2005) and Popov (Popov 2011) was adopted. This scheme includes 13 species such as e^-, N_2, $N_2(C^3\Pi_u)$, $N_2(B^3\Pi_g)$, O_2, O, $O(^1D)$, and 38 reactions. The Poisson equation and Helmholtz equation were solved by a preconditioned conjugate-gradient solver. For the initial and boundary conditions we adopted the scheme proposed by Zhu (Zhu et al., 2017).

3. Results and discussion

3.1. Disinfection performance of lgDBD

The disinfection efficiency of lgDBD was evaluated across varying voltage conditions. Fig. 1a displays the log inactivation efficiency for *Pseudomonas fluorescens*. At 9 kV, *Pseudomonas fluorescens* exhibited a reduction of approximately 6.4-log in 10 min. As the voltage increased to 12 kV, the inactivation efficiency significantly improved, with complete inactivation of *Pseudomonas fluorescens* achieved within 8 min (>7.0-log). The behaviour of *Bacillus subtilis*, the Gram-positive model bacteria, was similar to that of *Pseudomonas fluorescens* in the same lgDBD setup with different applied voltages (Fig. 1b). Compared to *Pseudomonas fluorescens,* LgDBD demonstrated higher inactivation efficiency against *Bacillus subtilis* because *Bacillus subtilis* exhibited greater sensitivity to ozone (Wang et al., 2021a). Given its effective disinfection against both Gram-negative and Gram-positive bacteria, plasma discharge technique has the potential to address many waterborne microbial disinfection challenges.

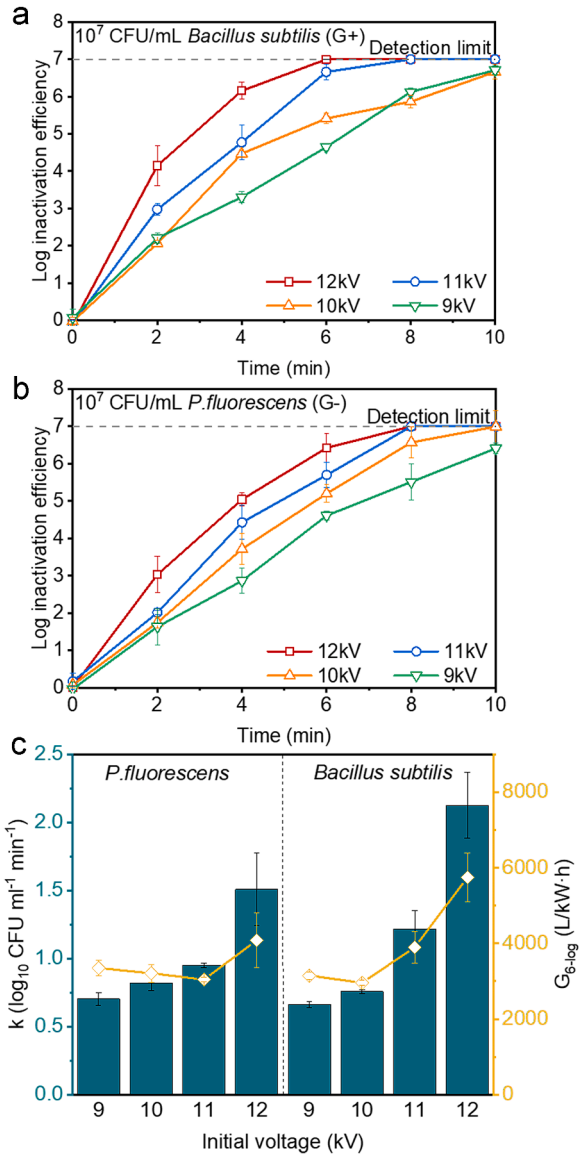

Fig. 1. Logarithmic inactivation efficiency of (a) *Pseudomonas fluorescens* and (b) *Bacillus subtilis* under various initial voltages; Conditions: bacterial initial concentration: 10^7 CFU/mL; pH: 7.0. (c)Pseudo-first-order inactivation rate constants and energy efficiencies at different initial voltages.

Further analysis was conducted on the pseudo-first-order bacterial inactivation rate constant and energy efficiency across various voltage conditions, as depicted in Fig. 1c. Consistent with the above disinfection efficiency findings, a surge in voltage corresponded to an increase in the pseudo-first-order inactivation rate constant. Here, $G_{6\text{-log}}$ indicates the volume of water disinfected to an efficiency of 6.0-log per unit of electricity used. At 12 kV, the sterilization energy efficiency peaked: $G_{6\text{-log}}$ values reached 4080.18 L/kWh for *Pseudomonas fluorescens* and 5745.95 L/kWh for *Bacillus subtilis*. This heightened energy efficiency at increased voltage is thought to stem from electroporation triggered by the powerful electric field and the impact of ROS and RNS (Chen et al., 2023; Deng et al., 2023; Li et al., 2023). Later sections will offer a more in-depth exploration of these components and their significance in the sterilization process. Table S1 provides a comparative analysis of the lgDBD and prevalent disinfection techniques, including O_3, Cl_2, and UV that spans three key parameters: inactivation efficiency, energy (oxidant) input, and E_{EO}. Notably, for the lgDBD method, the E_{EO} values for the removal of *Pseudomonas fluorescens* and *Bacillus subtilis* were 0.292 kWh m^{-3} and 0.264 kWh m^{-3}, respectively. In contrast, the E_{EO} values for O_3 were significantly lower than for lgDBD, at 0.848 kWh m^{-3} (*Pseudomonas fluorescens*) and 0.706 kWh m^{-3} (*Bacillus subtilis*), respectively. Similarly, the E_{EO} values of lgDBD were also advantageous relative to UV (260, 280 nm). According to previous studies, an E_{EO} value of less than 1 kWh m^{-3} indicates a range feasible for comprehensive practical application (Moreno-Andrés et al., 2023). Therefore, lgDBD demonstrates strong potential for practical application in terms of energy consumption.

The inactivation efficiency of lgDBD for *Bacillus subtilis* exceeded 99.99999 % (>7.0-log). By contrast, when given an identical energy input of 18.5 W, the inactivation efficiency of O_3 (3.29-log) is significantly lower than that of lgDBD. Notably, the inactivation efficiency of the lgDBD method gives it a compelling advantage over various other disinfection methods.

3.2. Feasibility of lgDBD in different conditions

The disinfection efficacy of plasma discharge was assessed across various gas compositions, including air, nitrogen, and noble gases. As depicted in Fig. S2, under a nitrogen atmosphere, the pseudo-first-order rate constant for sterilization was distinctly lower than with other gases. However, the disinfection efficiency between air and noble gases such as Ne and Ar showed negligible differences. While noble gas discharges are molecular, primarily producing excited states of the respective gases, air discharges are ionic (Guo et al., 2021; Liu et al., 2023; Zhang et al., 2022). This means that air not only yields excited states of nitrogen and oxygen but also generates gaseous ROS and RNS (Liu et al., 2022b; Zhu et al., 2017). Previous research has indicated that in perfluorooctanoic acid plasma treatment, the degradation rates using Ne and Ar discharges exceed those from air discharges (Zhang et al., 2021). Although the reactive species produced by rare gas discharge and air discharge differ, they exhibit similar disinfection efficiencies. Economically speaking, air represents the most feasible gaseous environment for plasma discharge sterilization.

Long-term disinfection results are shown in Fig. S3. Throughout the 10 cycles, lgDBD consistently maintained the same level of sterilization effectiveness. In fact, the sterilization effect in some later cycles was

even better than in the 1st, which could be due to the cumulative effect of temperature contributing to the sterilization. Fig. S4 illustrates that within a wide pH range of 3.0 to 11.0, both *Pseudomonas fluorescens* and *Bacillus subtilis* were be effectively eliminated, with reductions greater than 5.30-log and 5.58-log in 6 min, respectively. A rising pH marginally diminishes the inactivation efficiency of the lgDBD system. Ozone exhibits increased solubility in conditions of lower pH, and an alkaline environment also promotes the quenching of ·OH (Wu et al., 2020). 1.0 mg/L humic acid (HA) concentration did not notably hinder the inactivation process (Fig. S5). However, 10.0 mg/L HA concentration showed a minor reduction in inactivation efficiency, achieving over 5.35-log in 6 min.

The disinfection efficiency of lgDBD was further examined in real water samples. Table S2 lists the main properties of these experimental water samples. In lake and river water, the inactivation rates of *Pseudomonas fluorescens* and *Bacillus subtilis* slightly decreased compared to pure water (as shown in Fig. S6). In secondary effluent, the bacterial inactivation rate was significantly impacted. Although the electric field effect of lgDBD functioned normally in all the different water samples, the sterilizing effect of the reactive species was impacted negatively due to the competitive action of organic matter. The negative correlation between the chemical oxygen demand of the water samples and the sterilization rate confirms this. Nevertheless, a reduction of over 5.58-log in bacteria was observed within 6 min in real water samples, indicating that the lgDBD process has the potential to mitigate microbial health issues in complex water samples.

Additionally, due to its energy efficiency (E_{EO} 0.264–0.292 kWh m^{-3}), the lgDBD process holds promise for preliminary large-scale applications, though there are still challenges. With the scaling up of any lgDBD device, the stability of discharge becomes a critical issue that needs to be addressed. Instability in local water flow can disrupt the uniformity of global discharge. To address this, using multiple devices in parallel is an effective method to control risks. Setting up guide channels can also help enhance the stability of water flow in the discharge area.

3.3. Bacterial membrane damage

SEM was utilized to observe morphological changes in *Bacillus subtilis* and *Pseudomonas fluorescens* before and after plasma discharge treatment. The microscopy revealed surface and structural modifications in the bacterial cells at different stages of the experiment. Specifically, untreated bacterial samples showcased a smooth and intact rod-like appearance (refer to Fig. 2a, d). However, after 5 to 10 min of plasma discharge treatment, prominent cellular damage became evident, with observable indentations (Fig. 2b), punctures (Fig. 2e), distortions, and breaks (Fig. 2c, f). These microscopic images provide visual evidence for

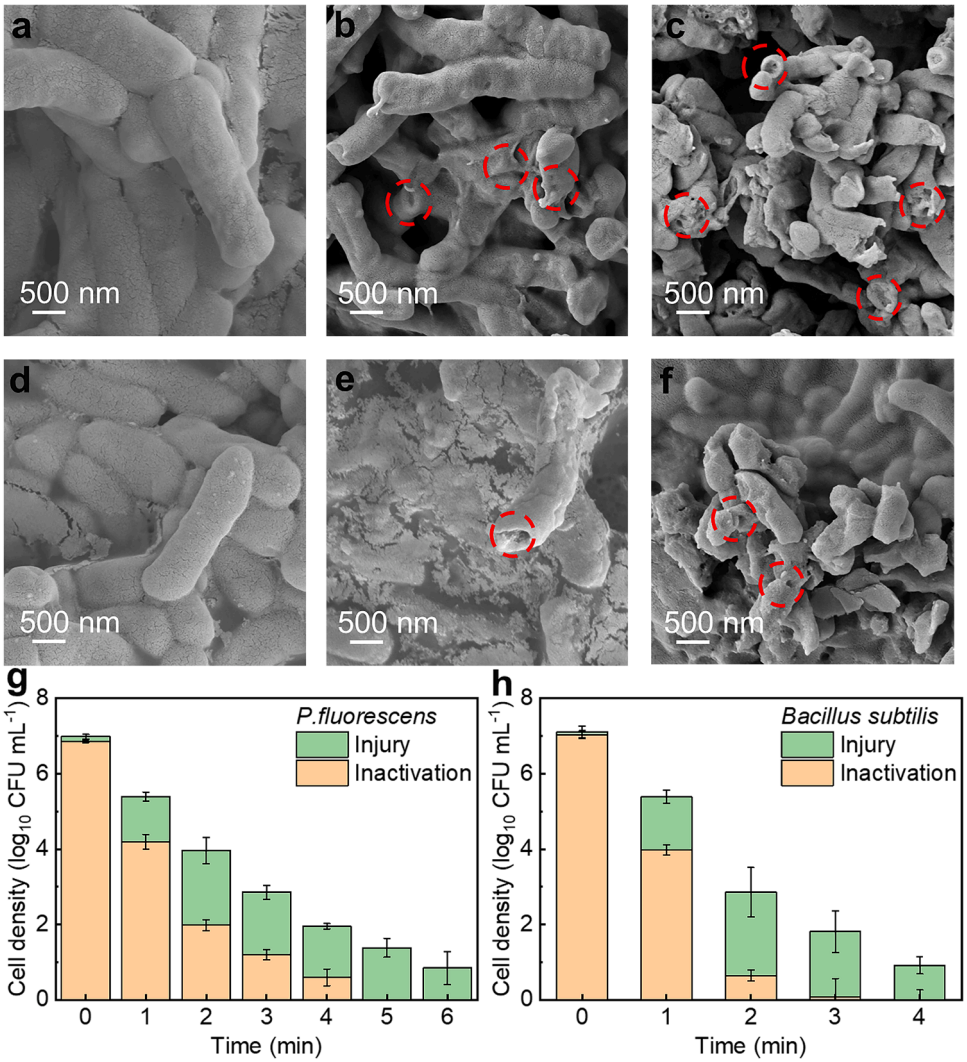

Fig. 2. Scanning electron micrographs of *Bacillus subtilis* (a) in their untreated state, (b) after 5 min of treatment, (c) after 10 min of treatment; Scanning electron micrographs of *Pseudomonas fluorescens* (d) in their untreated state, (e) after 5 min of treatment, (f) after 10 min of treatment; Injury and inactivation status of (g) *Pseudomonas fluorescens* and (h) *Bacillus subtilis* under 12 kV conditions.

the impact of plasma discharge on the bacteria (He et al., 2021; Nguyen et al., 2021; Shen et al., 2023).

Plasma discharge is theorized to inactivate bacteria by producing ROS such as ozone and hydroxyl radicals (Nie et al., 2013; Singh et al., 2019a), but the cell membrane damage, as seen through SEM, may also originate from the powerful electric field (Zhou et al., 2020). The 5 % NaCl stress selection experiment further confirmed the sublethal injury condition of bacteria caused by cell membrane damage (Fig. 2g, h). Post lgDBD treatment, between 83.84 % and 99.37 % of *Pseudomonas fluorescens* and *Bacillus subtilis* were found to be in an 'injured' state (able to survive in a nutrient broth, but not in one with 5 % NaCl). This evidence suggests that the lgDBD treatment inflicts significant damage to the bacterial cell membrane that leads to bacterial inactivation.

To delve deeper into the mechanism of bacterial inactivation during lgDBD treatment, we also utilized flow cytometry combined with SYTO™ 9 and PI staining. This approach quantifies both bacterial inactivation and cellular membrane damage. SYTO™ 9 interacts with the deoxyribonucleic acid (DNA) of viable bacteria, producing a green fluorescence, and PI targets the DNA of bacteria whose cell membranes have been compromised, resulting in a red fluorescence (Qi et al., 2022). Consequently, the flow cytometry results can be divided into four quadrants: the first quadrant represents live bacteria with damaged membranes, the second quadrant indicates inactivated bacteria, the third captures impurities, and the fourth signifies live bacteria with intact membranes (Zhou et al., 2020). As illustrated in Fig. 3a-f, post-plasma discharge treatment resulted in a decrease in the bacteria percentage within the fourth quadrant. In contrast, there was a noticeable increase in the first and second quadrants. These findings indicate that lgDBD treatment severely damages bacterial cell membranes, prompting their inactivation (Lu et al., 2023; Lukes et al., 2014). Supporting visual evidence can be observed in the confocal microscopy images presented in Fig. 3g-j and Fig. S7.

3.4. Basic discharge unit model

Previous research held that UV and reactive species like O_3 and ·OH made significant contributions to the sterilization of lgDBD, however overlooked the role of the electric field (Patinglag et al., 2021). Given that the duration of a single discharge typically lasts less than 100 nanoseconds, conventional diagnostic tools for discharge plasma, including intensified charge-coupled device (ICCD) imaging and OES spectral analysis, struggle to discern the physicochemical attributes of the basic discharge unit, limiting research on electric field sterilization (Popov 2011; Singh et al., 2019b; Zhou et al., 2020). In order to addressing this limitation, we employed 2D PASSKEy code, which integrates fluid dynamics, to simulate the basic discharge unit (Yin et al., 2023).This model derives solutions for electric field intensity, electron density, and various component concentrations by integrating continuity equations in discharge chemical kinetics with the Poisson equation. As to the validity of the model, the consistency between the model and

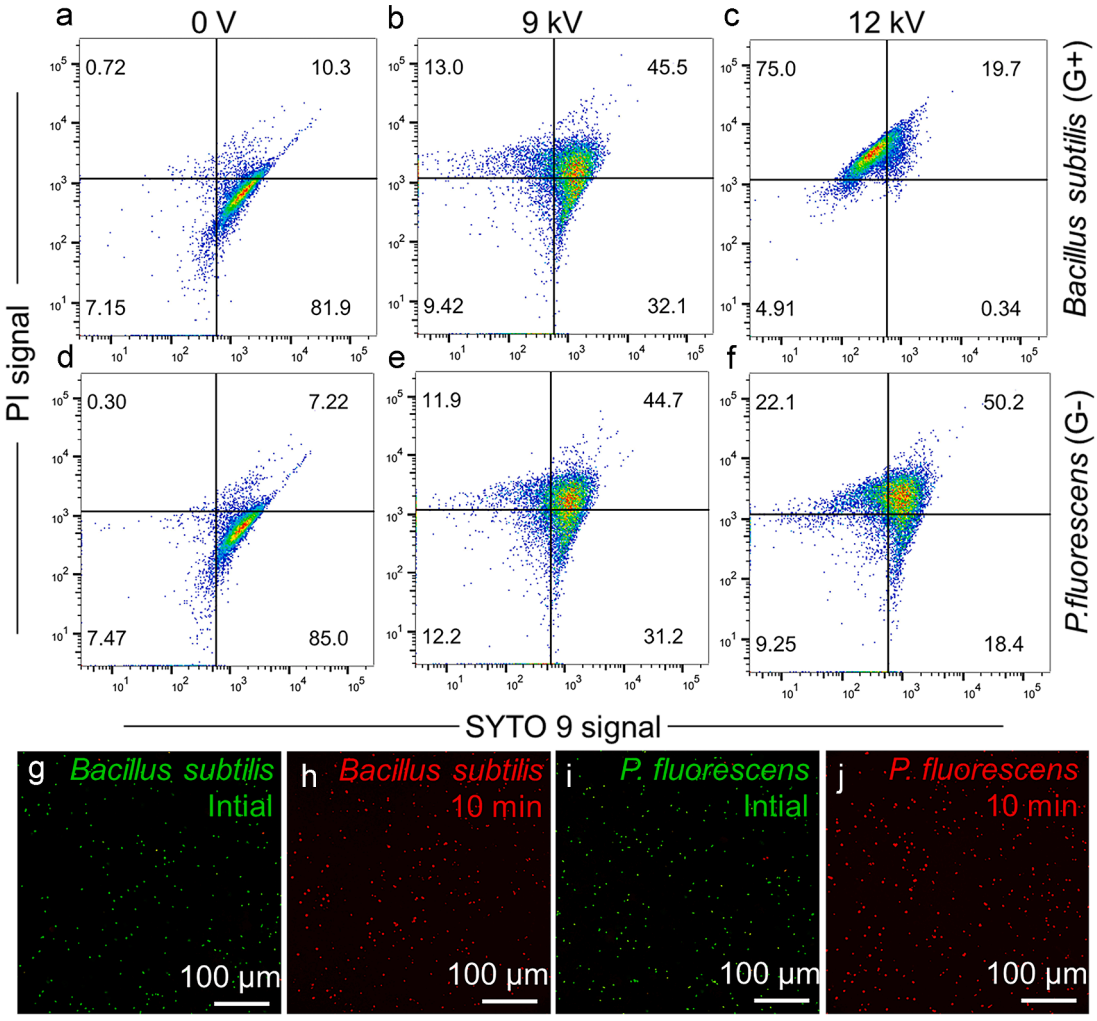

Fig. 3. Flow cytometry analysis of (a-c) *Bacillus subtilis* and (d-f) *Pseudomonas fluorescens* after treatment with discharge plasma and dual-staining with SYTO™ 9 and PI; Co-localization images of (g-h) *Bacillus subtilis* and (i-j) *Pseudomonas fluorescens* obtained through dual-staining with SYTO™ 9 and PI using confocal microscopy.

the benchmark case has already been demonstrated in previous studies (Lukes et al., 2014), and the composition of excited state substances and long-lived reactive species in the model and experiment are compared in later sections.

Simulation results demonstrate that the basic discharge unit of lgDBD has a cumulative duration of 9.94 × 10^{-9} seconds, and the distribution of free electrons can be observed in Fig. 4b, Fig. S8d-f, and Video S1. These free electron concentration distributions indicate the propagation of the plasma. Each basic discharge unit progresses through four stages: the initiation of seed electrons, the electron avalanche, streamer propagation, and the post-conduction spark discharge (Zhu et al., 2017). These phases cease when a transition to a thermally stable arc is not achievable, resulting in repeated cycles. During each basic discharge unit, an electric field ranging from 4.77 × 10^4 to 2.86 × 10^6 V/m is generated that coincides with the spread of the plasma streamer (Fig. 4c, Fig. S8a-c, and Video S2). It is noteworthy that the strongest electric field continuously exists near the surface of the liquid during the propagation of the streamer. This is because, during the propagation of the streamer, the positive ions and free electrons in the plasma move in opposite directions under the action of the electrode electric field. This leads to a local charge imbalance at the head and tail of the plasma, forming a responsive electric field far stronger than the intensity of the electrode electric field itself (Adamovich et al., 2022). Previous research has established that an electric field intensity of 1.0 × 10^6 V/m is capable of triggering lethal electroporation in bacterial cells (Wang et al., 2022a, Zhou et al., 2020). Therefore, lgDBD can generate a sufficiently strong electric field for sterilization purposes.

During the discharge, free electrons collide with oxygen and nitrogen molecules, producing excited state substances, positive ions, and more free electrons, which are the sources of the plasma reactive species (Popov, 2011). Based on our simulation, the primary reactive species produced during plasma discharge include oxygen atoms (which can merge with oxygen to produce ozone) and O(^{1}D). Their spatiotemporal distribution is shown in Fig. 4d-e, Fig. S8g-l, and Video S3–4. Oxygen atoms are generated uniformly along the plasma streamer propagation path, however O(^{1}D) is more concentrated at the tip of the streamer. The different behaviors of the two particles may stem from the differences in their lifespans (Zhu et al., 2017). The reactive species produced by the discharge react at the gas-liquid boundary on one hand, generating ROS in the liquid phase, and on the other hand, some dissolve in water, enhancing the sterilization of lgDBD (Ma et al., 2022; Nahim-Granados et al., 2020).

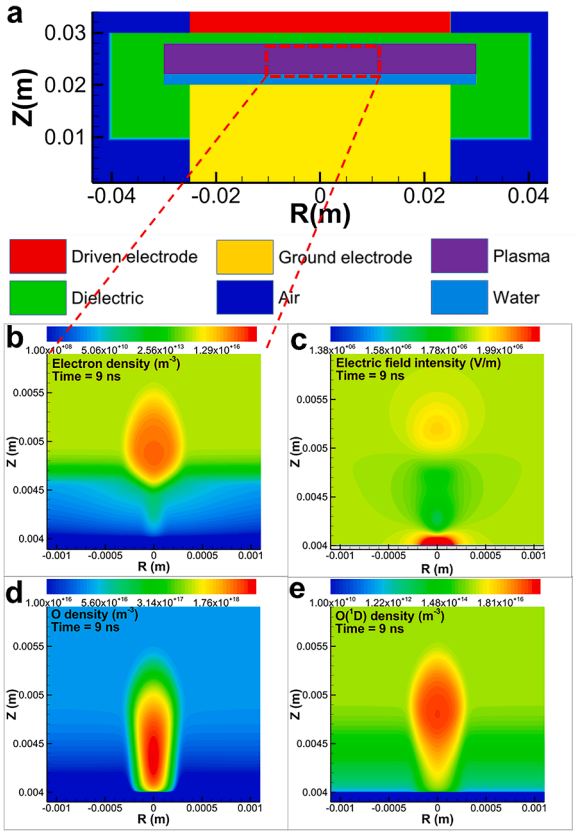

Fig. 4. The basic discharge unit model using PASSKEy code. (a) Geometric setting, (b) electron density, (c) electric field, (d) oxygen density, and (e) O (^{1}D) density.

3.5. Identification of reactive species

Fig. 5a, which illustrates by the OES spectroscopy, shows that oxygen and nitrogen in their excited states are the primary gaseous reactive species during lgDBD treatment. Notably, two excited states of N_2 [$N_2(C^3\Pi_u)$ and $N_2(B^3\Pi_g)$] are represented (Guo et al., 2021; Tang et al., 2023). This suggests the presence of an active second positive system (SPS) of nitrogen in the discharge plasma, consistent with the results from the plasma discharge simulation (Fig. S10 and Fig. S11). Additionally, peaks at 291.2 nm and 777.4 nm indicate the presence of NO and oxygen atoms, respectively. It is noteworthy that there was also a suspected blue shift in the OES spectrum, which may be caused by the refraction of the quartz glass layer during the measurement process. There is also a focus on long-lived reactive species in water (Fig. 5b). As voltage increases, so do the concentrations of nitrate ions (reflecting the RNS content in water) and H_2O_2. Higher voltages generate more reactive species than lower voltages. However, an anomaly was observed at 12 kV, where ozone levels decrease compared to those at 11 kV. This decline might be due to the thermal effects from the increased voltage, causing ozone degradation (Wu et al., 2020). Additionally, previous research suggests that lower voltage discharges lean towards an ozone-centric mode and that higher voltages shift to a nitrogen oxide mode, which could explain this observation (Zhu et al., 2023). Furthermore, when bacteria were added to the solution, the accumulation concentration of nitrate decreased, and this was because the bacteria consumed the reactive species, resulting in interference with the production of RNS.

EPR testing was used to examine the short-lived reactive species produced by lgDBD. Fig. 5c shows the characteristic adduct signals of ·OH with DMPO in lgDBD, indicating the production of ·OH in the aqueous phase during the discharge (Farinelli et al., 2021; Tang et al., 2023). According to the basic discharge unit model, the discharge produces abundant O and O_3 in the gas phase that dissolve and react at the gas-liquid interface to form ROS in the liquid phase. As shown in Fig. 5d, the characteristic signal with a peak ratio of 1:1:1 indicates the presence of $^1O_2$, which is the excited state of oxygen. The basic discharge unit model also shows that the discharge products contain excited state oxygen atoms such as O(^{1}D), which may be the direct source of $^1O_2$ in the liquid phase. When bacterial fluid was introduced, the peaks corresponding to each reactive oxygen species disappeared. This implies that ·OH, and $^1O_2$ all play roles in bacterial inactivation.

Based on the above results, a generation pathway for reactive species in lgDBD has been hypothesized. Plasma discharge occurs in air, with the generation of a large number of free electrons being its most significant characteristic (Adamovich et al., 2017). These free electrons have an extremely short lifespan and, upon colliding with molecules such as O_2 and N_2, produce excited state species such as O(^{1}D), $N_2(C^3\Pi_u)$, and $N_2(B^3\Pi_g)$, as well as ROS such as oxygen atoms and O_3 (Zhu et al., 2017), which is confirmed by the basic discharge unit model and OES. These substances dissolve and react at the gas-liquid interface, forming reactive species in the liquid phase. $N_2(C^3\Pi_u)$ and $N_2(B^3\Pi_g)$ may form RNS such as ONOOH, and oxygen atoms, O_3, and O(^{1}D) generate ROS such as ·OH, and $^1O_2$ in the liquid phase (Adamovich et al., 2022). The combined action of these reactive species and the electric field effect

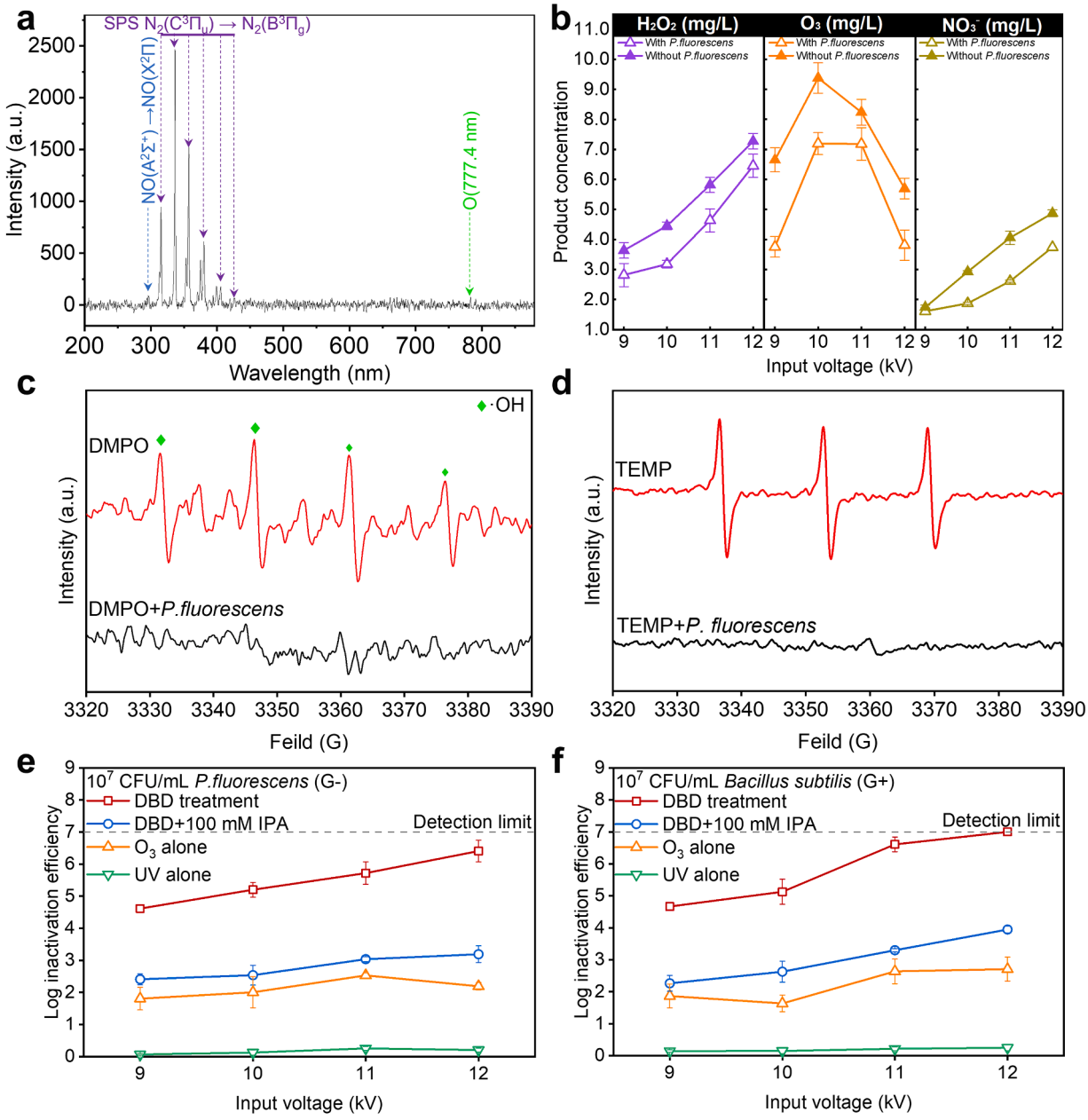

Fig. 5. (a) Optical emission spectra during plasma discharge; (b) The generation of hydrogen peroxide, ozone, and nitrate ions during plasma discharge; EPR spectra using (c) DMPO and (d) TEMP. The logarithmic inactivation efficiencies of (e) *Pseudomonas fluorescens* and (f) *Bacillus subtilis* under various treatment conditions; Conditions: bacterial initial concentration: 10^7 CFU/mL; time = 6 min.

leads to the inactivation of bacteria.

3.6. Mechanisms of bacteria inactivation

The lgDBD process involves elements such as electric fields, reactive species, and UV radiation that can each potentially lead to bacterial inactivation. To understand the role of each of these elements in sterilization, we evaluated inactivation efficiency under various conditions. Details of the experimental setup can be found in Text S2. Fig. 5e, f shows that O_3 led to significant deactivation in *Pseudomonas fluorescens* (from 1.71 to 2.52-log) and *Bacillus subtilis* (from 1.58 to 2.62-log). Additionally, in order to assess the respective contributions of electroporation and reactive species oxidation to bacterial disinfection, an excess of reactive species neutralizer (100 mM isopropanol (IPA)) was introduced (Tang et al., 2023). The results showed a decrease in sterilization effectiveness by 2.34 to 4.06-log, reflecting the significant contribution of reactive species oxidation to the sterilization process. Moreover, even in the presence of an excess of reactive species neutralizer, lgDBD still achieved 2.22 to 3.94-log bacterial inactivation. This indicates that electroporation, primarily as a non-reactive species effect, is also an important component of the sterilization efficacy of lgDBD. Especially, UV radiation had a negligible effect on sterilization, contributing to less than 0.25-log reduction. Combined with the simulation results of lgDBD, it is evident that electric field-induced electroporation is a key factor in the sterilization ability of nonreactive species.

Our findings reveal that lgDBD deactivates bacteria by harnessing both the physical mechanisms of electroporation and the chemical oxidation actions driven by ROS and RNS. During lgDBD treatment, the streamer propagation process in each basic discharge unit leads to the formation of a strong electric field, instigating bacterial electroporation. This action compromises the integrity of the bacterial cell membrane, prompting the leakage of intracellular contents and enabling ROS and

RNS penetration. Once inside, these ROS and RNS attack vital biomacromolecules such as proteins and DNA, further obstructing the ability of bacteria to repair from otherwise reversible electroporation. Consequently, when contrasted with ozonation, lgDBD introduces an auxiliary electroporation disinfection pathway, thereby achieving superior disinfection efficiency with equivalent energy consumption.

4. Conclusion

In this work, lgDBD was used for the disinfection of DRB. After a 12 kV discharge treatment, *Bacillus subtilis* and *Pseudomonas fluorescens* were inactivated over 7.0-log within 6 and 8 min, respectively. Inactivation capacity of DRB was successfully tested across a wide range of pH values and various actual water samples, demonstrating the broad applicability of lgDBD. Bacterial response analysis also indicated that cell membrane damage was the primary cause of bacterial inactivation. By constructing a basic discharge unit model based on the PASSKEy code, it was proven that the responsive electric field during streamer propagation amplified the inherent electric field, reaching the sterilization threshold. Combined with reactive species analysis, it was shown that electric field-induced electroporation as well as oxidation by reactive oxygen and nitrogen species were the greatest sources of bacterial inactivation. Overall, this study shows that lgDBD can efficiently inactivate DRB, providing new insights into the practical application of physicochemical synergistic sterilization technology in water treatment.

Supporting information

Supplementary texts, tables, figures and videos can be found online.

Additional experimental details and methods, including chemicals, reagents, microbial cultures, experimental setup, and data handling; a schematic diagram of the lgDBD treatment; logarithmic inactivation efficiency of *Pseudomonas fluorescens* and *Bacillus subtilis* with different gases, pH values, dosages of HA, and water substrates; electric field, electron density, oxygen density, $O(^1D)$ density, E/N, $N_2(C^3\Pi_u)$, and $N_2(B^3\Pi_g)$ of the basic discharge unit model using the PASSKEy code; and inactivation efficiency of several target microorganisms and import in different treatment methods (DOC).

Video S1. The spatiotemporal variation of electron density during discharge (MP4).

Video S2. The spatiotemporal variation of electric field during discharge (MP4).

Video S3. The spatiotemporal variation of oxygen density during discharge (MP4).

Video S4. The spatiotemporal variation of $O(^1D)$ density during discharge (MP4).

CRediT authorship contribution statement

Ruoyu Deng: Writing – review & editing, Writing – original draft, Visualization, Software, Data curation, Conceptualization. **Qiang He:** Writing – review & editing, Validation, Supervision, Project administration, Funding acquisition. **Dongxu Yang:** Writing – review & editing, Supervision. **Mengli Chen:** Writing – review & editing, Validation. **Yi Chen:** Writing – review & editing, Visualization, Validation, Resources, Project administration, Conceptualization.

Declaration of competing interest

The authors declare that they have no known competing financial interests or personal relationships that could have appeared to influence the work reported in this paper.

Data availability

Data will be made available on request.

Acknowledgments

This work was funded by the Chongqing Talents Plan for Young Talents (CQY201905062) and the Chongqing Science Fund for Distinguished Young Scholars (CSTB2022NSCQ-JQX0023). The authors thank the Analytical and Testing center of Chongqing University and Shiyanjia Lab (www.shiyanjia.com) for various tests. The authors thank AiMi Academic Services (www.aimieditor.com) for English language editing and review services.

Supplementary materials

Supplementary material associated with this article can be found, in the online version, at doi:10.1016/j.watres.2024.121386.

References

Adamovich, I., Agarwal, S., Ahedo, E., Alves, L.L., Baalrud, S., Babaeva, N., Bogaerts, A., Bourdon, A., Bruggeman, P.J., Canal, C., Choi, E.H., Coulombe, S., Donkó, Z., Graves, D.B., Hamaguchi, S., Hegemann, D., Hori, M., Kim, H.H., Kroesen, G.M.W., Kushner, M.J., Laricchiuta, A., Li, X., Magin, T.E., Thagard, S.M., Miller, V., Murphy, A.B., Oehrlein, G.S., Puac, N., Sankaran, R.M., Samukawa, S., Shiratani, M., Simek, M., Tarasenko, N., Terashima, K., Thomas, E., Trieschmann, J., Tsikata, S., Turner, M.M., van der Walt, I.J., van de Sanden, M.C.M., von Woedtke, T., 2022. The 2022 Plasma Roadmap: low temperature plasma science and technology. J. Phys. D-Appl. Phys. 55 (37).

Adamovich, I., Baalrud, S.D., Bogaerts, A., Bruggeman, P.J., Cappelli, M., Colombo, V., Czarnetzki, U., Ebert, U., Eden, J.G., Favia, P., Graves, D.B., Hamaguchi, S., Hieftje, G., Hori, M., Kaganovich, I.D., Kortshagen, U., Kushner, M.J., Mason, N.J., Mazouffre, S., Thagard, S.M., Metelmann, H.R., Mizuno, A., Moreau, E., Murphy, A. B., Niemira, B.A., Oehrlein, G.S., Petrovic, Z.L., Pitchford, L.C., Pu, Y.K., Rauf, S., Sakai, O., Samukawa, S., Starikovskaia, S., Tennyson, J., Terashima, K., Turner, M. M., van de Sanden, M.C.M., Vardelle, A., 2017. The 2017 Plasma Roadmap: low temperature plasma science and technology. J. Phys. D-Appl. Phys. 50 (32).

Aka, R.J.N., Wu, S., Mohotti, D., Bashir, M.A., Nasir, A., 2022. Evaluation of a liquid-phase plasma discharge process for ammonia oxidation in wastewater: process optimization and kinetic modeling. Water Res. 224, 119107.

Cao, K.-F., Chen, Z., Sun, Y.-G., Huang, B.-H., Shi, Q., Mao, Y., Wu, Y.-H., Lu, Y., Hu, H.-Y., 2023. Modeling and optimization of synergistic ozone-ultraviolet-chlorine process for reclaimed water disinfection: from laboratory tests to software simulation. Water Res. 243, 120373.

Chen, C., Ma, C., Yang, Y., Yang, X., Demeestere, K., Nikiforov, A., Van Hulle, S., 2023. Degradation of micropollutants in secondary wastewater effluent using nonthermal plasma-based AOPs: the roles of free radicals and molecular oxidants. Water Res. 235, 119881.

Deng, R., He, Q., Yang, D., Dong, Q., Wu, J., Yang, X., Chen, Y., 2021. Enhanced synergistic performance of nano-Fe0-CeO2 composites for the degradation of diclofenac in DBD plasma. Chem. Eng. J. 406, 126884.

Deng, R., Yang, D., Chen, M., He, Q., He, Q., Chen, Y., 2023. The enhancing energy efficiency of sulfadiazine degradation using a DBD-contact plasma treatment process. Chem. Eng. J. 463, 142491.

El-Athman, F., Zehlike, L., Kämpfe, A., Junek, R., Selinka, H.-C., Mahringer, D., Grunert, A., 2021. Pool water disinfection by ozone-bromine treatment: assessing the disinfectant efficacy and the occurrence and in vitro toxicity of brominated disinfection by-products. Water Res. 204, 117648.

Farinelli, G., Giagnorio, M., Ricceri, F., Giannakis, S., Tiraferri, A., 2021. Evaluation of the effectiveness, safety, and feasibility of 9 potential biocides to disinfect acidic landfill leachate from algae and bacteria. Water Res. 191, 116801.

Guo, H., Jiang, N., Wang, H., Shang, K., Lu, N., Li, J., Wu, Y., 2019. Enhanced catalytic performance of graphene-TiO2 nanocomposites for synergetic degradation of fluoroquinolone antibiotic in pulsed discharge plasma system. Appl. Catal. B 248, 552–566.

Guo, H., Pan, S., Hu, Z., Wang, Y., Jiang, W., Yang, Y., Wang, Y., Han, J., Wu, Y., Wang, T., 2023. Persulfate activated by non-thermal plasma for organic pollutants degradation: a review. Chem. Eng. J. 470.

Guo, L., Yao, Z., Yang, L., Zhang, H., Qi, Y., Gou, L., Xi, W., Liu, D., Zhang, L., Cheng, Y., Wang, X., Rong, M., Chen, H., Kong, M.G., 2021. Plasma-activated water: an alternative disinfectant for S protein inactivation to prevent SARS-CoV-2 infection. Chem. Eng. J. 421.

He, J., Zheng, Z., Lo, I.M.C., 2021. Different responses of gram-negative and gram-positive bacteria to photocatalytic disinfection using solar-light-driven magnetic TiO2-based material, and disinfection of real sewage. Water Res. 207, 117816.

Hogard, S., Pearce, R., Gonzalez, R., Yetka, K., Bott, C., 2023. Optimizing ozone disinfection in water reuse: controlling bromate formation and enhancing trace organic contaminant oxidation. Environ. Sci. Technol.

Huo, Z.-Y., Winter, L.R., Wang, X.-X., Du, Y., Wu, Y.-H., Hübner, U., Hu, H.-Y., Elimelech, M., 2022. Synergistic nanowire-enhanced electroporation and electrochlorination for highly efficient water disinfection. Environ. Sci. Technol. 56 (15), 10925–10934.

Huo, Z.-Y., Yang, Y., Jeong, J.-M., Wang, X., Zhang, H., Wei, M., Dai, K., Xiong, P., Kim, S.-W., 2023a. Self-powered disinfection using triboelectric, conductive wires of metal–organic frameworks. Nano Lett. 23 (7), 3090–3097.
Huo, Z.Y., Kim, Y.J., Chen, Y.Y., Song, T.Y., Yang, Y., Yuan, Q.B., Kim, S.W., 2023b. Hybrid energy harvesting systems for self-powered sustainable water purification by harnessing ambient energy. Front. Environ. Sci. Eng. 17 (10).
Jung, Y.J., Oh, B.S., Kang, J.-W., 2008. Synergistic effect of sequential or combined use of ozone and UV radiation for the disinfection of Bacillus subtilis spores. Water Res. 42 (6), 1613–1621.
Li, R., Isowamwen, O.F., Ross, K.C., Holsen, T.M., Thagard, S.M., 2023. PFAS–CTAB complexation and its role on the removal of PFAS from a lab-prepared water and a reverse osmosis reject water using a plasma reactor. Environ. Sci. Technol.
Liu, F., Li, Z., Dong, Q., Nie, C., Wang, S., Zhang, B., Han, P., Tong, M., 2022a. Catalyst-free periodate activation by solar irradiation for bacterial disinfection: performance and mechanisms. Environ. Sci. Technol. 56 (7), 4413–4424.
Liu, Y., Duan, J., Zhou, Q., Zhu, L., Liu, N., Sun, Z., 2023. Effective degradation of lindane and its isomers by dielectric barrier discharge (DBD) plasma: synergistic effects of various reactive species. Chemosphere 338, 139607. -139607.
Liu, Y., Li, H., Wang, R., Hu, Q., Zhang, Y., Wang, Z., Zhou, J., Qu, G., Wang, T., Jia, H., Zhu, L., 2022b. Underlying mechanisms of promoted formation of haloacetic acids disinfection byproducts after indometacin degradation by non-thermal discharge plasma. Water Res. 220, 118701.
Lu, Y.-W., Liang, X.-X., Wang, C.-Y., Chen, D., Liu, H., 2023. Synergistic nanowire-assisted electroporation and chlorination for inactivation of chlorine-resistant bacteria in drinking water systems via inducing cell pores for chlorine permeation. Water Res. 229, 119399.
Lukes, P., Dolezalova, E., Sisrova, I., Clupek, M., 2014. Aqueous-phase chemistry and bactericidal effects from an air discharge plasma in contact with water: evidence for the formation of peroxynitrite through a pseudo-second-order post-discharge reaction of H2O2 and HNO2. Plasma Sources Sci. Technol. 23 (1).
Luo, L.-W., Wu, Y.-H., Yu, T., Wang, Y.-H., Chen, G.-Q., Tong, X., Bai, Y., Xu, C., Wang, H.-B., Ikuno, N., Hu, H.-Y., 2021. Evaluating method and potential risks of chlorine-resistant bacteria (CRB): a review. Water Res. 188, 116474.
Ma, B., Seyedi, S., Wells, E., McCarthy, D., Crosbie, N., Linden, K.G., 2022. Inactivation of biofilm-bound bacterial cells using irradiation across UVC wavelengths. Water Res. 217.
Mao, X., Zhong, H., Zhang, T., Starikovskiy, A., Ju, Y., 2022. Modeling of the effects of non-equilibrium excitation and electrode geometry on H2/air ignition in a nanosecond plasma discharge. Combust. Flame 240, 112046.
Moreno-Andrés, J., Tierno-Galán, M., Romero-Martínez, L., Acevedo-Merino, A., Nebot, E., 2023. Inactivation of the waterborne marine pathogen Vibrio alginolyticus by photo-chemical processes driven by UV-A, UV-B, or UV-C LED combined with H2O2 or HSO5−. Water Res. 232, 119686.
Morrison, C.M., Hogard, S., Pearce, R., Gerrity, D., von Gunten, U., Wert, E.C., 2022. Ozone disinfection of waterborne pathogens and their surrogates: a critical review. Water Res. 214, 118206.
Nahim-Granados, S., Rivas-Ibáñez, G., Antonio Sánchez Pérez, J., Oller, I., Malato, S., Polo-López, M.I., 2020. Synthetic fresh-cut wastewater disinfection and decontamination by ozonation at pilot scale. Water Res. 170, 115304.
Nau-Hix, C., Multari, N., Singh, R.K., Richardson, S., Kulkarni, P., Anderson, R.H., Holsen, T.M., Thagard, S.M., 2021. Field demonstration of a pilot-scale plasma reactor for the rapid removal of poly- and perfluoroalkyl substances in groundwater. ACS ES&T Water 1 (3), 680–687.
Nguyen, D.B., Matyakubov, N., Saud, S., Heo, I., Kim, S.-J., Kim, Y.J., Lee, J.H., Mok, Y. S., 2021. High-throughput NOx removal by two-stage plasma honeycomb monolith catalyst. Environ. Sci. Technol. 55 (9), 6386–6396.
Nie, Y., Zheng, Q., Liang, X., Gu, D., Lu, M., Min, M., Ji, J., 2013. Decomposition treatment of SO2F2 using packed bed DBD plasma followed by chemical absorption. Environ. Sci. Technol. 47 (14), 7934–7939.
Pak, G., Salcedo, D.E., Lee, H., Oh, J., Maeng, S.K., Song, K.G., Hong, S.W., Kim, H.-C., Chandran, K., Kim, S., 2016. Comparison of antibiotic resistance removal efficiencies using ozone disinfection under different pH and suspended solids and humic substance concentrations. Environ. Sci. Technol. 50 (14), 7590–7600.
Pancheshnyi, S., Nudnova, M., Starikovskii, A., 2005. Development of a cathode-directed streamer discharge in air at different pressures: experiment and comparison with direct numerical simulation. Phys. Rev. E 71 (1), 016407.
Patinglag, L., Melling, L.M., Whitehead, K.A., Sawtell, D., Iles, A., Shaw, K.J., 2021. Non-thermal plasma-based inactivation of bacteria in water using a microfluidic reactor. Water Res. 201, 117321.
Patinglag, L., Sawtell, D., Iles, A., Melling, L.M., Shaw, K.J., 2019. A microfluidic atmospheric-pressure plasma reactor for water treatment. Plasma Chem. Plasma Process. 39 (3), 561–575.
Pfaller, S., King, D., Mistry, J.H., Alexander, M., Abulikemu, G., Pressman, J.G., Wahman, D.G., Donohue, M.J., 2021. Chloramine concentrations within distribution systems and their effect on heterotrophic bacteria, mycobacterial species, and disinfection byproducts. Water Res. 205, 117689.
Popov, N.A., 2011. Fast gas heating in a nitrogen–oxygen discharge plasma: I. Kinetic mechanism. J. Phys. D Appl. Phys. 44 (28), 285201.
Qi, Z., Li, G., Wang, M., Chen, C., Xu, Z., An, T., 2022. Photoelectrocatalytic inactivation mechanism of E. coli DH5α (TET) and synergistic degradation of corresponding antibiotics in water. Water Res. 215.
Sharma, V.K., Zboril, R., Varma, R.S., 2015. Ferrates: greener oxidants with multimodal action in water treatment technologies. Acc. Chem. Res. 48 (2), 182–191.
Shen, T., Yu, H., Wang, P., Wang, X., Yang, C., Xu, P., Qu, J., Zhang, G., 2023. Layered double oxide/copper foam actuates dielectric barrier discharge plasma via electron transport: exploring the reactive species evolution and diuron disassembly routes. Appl. Catal. B 336, 122950.
Singh, R.K., Fernando, S., Baygi, S.F., Multari, N., Thagard, S.M., Holsen, T.M., 2019a. Breakdown products from perfluorinated alkyl substances (PFAS) degradation in a plasma-based water treatment process. Environ. Sci. Technol. 53 (5), 2731–2738.
Singh, R.K., Multari, N., Nau-Hix, C., Anderson, R.H., Richardson, S.D., Holsen, T.M., Mededovic Thagard, S., 2019b. Rapid removal of poly- and perfluorinated compounds from investigation-derived waste (IDW) in a pilot-scale plasma reactor. Environ. Sci. Technol. 53 (19), 11375–11382.
Singh, R.K., Multari, N., Nau-Hix, C., Woodard, S., Nickelsen, M., Mededovic Thagard, S., Holsen, T.M., 2020. Removal of poly- and per-fluorinated compounds from ion exchange regenerant still bottom samples in a plasma reactor. Environ. Sci. Technol. 54 (21), 13973–13980.
Stratton, G.R., Dai, F., Bellona, C.L., Holsen, T.M., Dickenson, E.R.V., Mededovic Thagard, S., 2017. Plasma-based water treatment: efficient transformation of perfluoroalkyl substances in prepared solutions and contaminated groundwater. Environ. Sci. Technol. 51 (3), 1643–1648.
Tang, Y., Zhang, H., Yan, J., Luo, N., Fu, X., Wu, X., Wu, J., Liu, C., Zhang, D, 2023. Assessing the efficacy of bleaching powder in disinfecting marine water: insights from the rapid recovery of microbiomes. Water Res. 241, 120136.
Van de Moortel, N., Van den Broeck, R., Degrève, J., Dewil, R., 2017. Comparing glow discharge plasma and ultrasound treatment for improving aerobic respiration of activated sludge. Water Res. 122, 207–215.
Wang, H.-B., Wu, Y.-H., Luo, L.-W., Yu, T., Xu, A., Xue, S., Chen, G.-Q., Ni, X.-Y., Peng, L., Chen, Z., Wang, Y.-H., Tong, X., Bai, Y., Xu, Y.-Q., Hu, H.-Y., 2021a. Risks, characteristics, and control strategies of disinfection-residual-bacteria (DRB) from the perspective of microbial community structure. Water Res. 204, 117606.
Wang, J., Chen, W., Wang, T., Reid, E., Krall, C., Kim, J., Zhang, T., Xie, X., Huang, C.-H., 2023a. Bacteria and virus inactivation: relative efficacy and mechanisms of peroxyacids and Chlor(am)ine. Environ. Sci. Technol.
Wang, R., Wang, T., Qu, G., Zhang, Y., Guo, X., Jia, H., Zhu, L., 2021b. Insights into the underlying mechanisms for integrated inactivation of A. spiroides and depression of disinfection byproducts by plasma oxidation. Water Res. 196, 117027.
Wang, S., Guan, B.Y., Wang, X., Lou, X.W.D., 2018. Formation of hierarchical Co_9S_8@ $ZnIn_2S_4$ heterostructured cages as an efficient photocatalyst for hydrogen evolution. J. Am. Chem. Soc. 140 (45), 15145–15148.
Wang, T., Brown, D.K., Xie, X., 2022a. Operando investigation of locally enhanced electric field treatment (LEEFT) harnessing lightning-rod effect for rapid bacteria inactivation. Nano Lett. 22 (2), 860–867.
Wang, Y., Jiang, W., Han, J., Qiao, W., Guo, H., 2023b. An in-depth insight into the simultaneous oxidation of sulfamethoxazole and reduction of Cr (VI) by one system of water film DBD plasma: the interaction effect, role of active species, and their dominant to pathways. Chemosphere 333.
Wang, Y., Yin, R., Tang, Z., Liu, W., He, C., Xia, D., 2022b. Reactive nitrogen species mediated inactivation of pathogenic microorganisms during UVA photolysis of nitrite at surface water levels. Environ. Sci. Technol. 56 (17), 12542–12552.
Waso, M., Khan, S., Singh, A., McMichael, S., Ahmed, W., Fernández-Ibáñez, P., Byrne, J. A., Khan, W., 2020. Predatory bacteria in combination with solar disinfection and solar photocatalysis for the treatment of rainwater. Water Res. 169, 115281.
Wu, G., Wang, J., Wan, Q., Cao, S., Huang, T., Lu, J., Ma, J., Wen, G., 2023. Kinetics and mechanism of sulfate radical-and hydroxyl radical-induced disinfection of bacteria and fungal spores by transition metal ions-activated peroxymonosulfate. Water Res. 243, 120378.
Wu, J., Xiong, Q., Liang, J., He, Q., Yang, D., Deng, R., Chen, Y., 2020. Degradation of benzotriazole by DBD plasma and peroxymonosulfate: mechanism, degradation pathway and potential toxicity. Chem. Eng. J. 384, 123300.
Yin, B., Zhu, Y., Wu, Y., 2023. Modulating sparks in a pulse train for repetitive and energy efficient plasma generation. High Voltage n/a(n/a).
Yu, Q., Wang, H., Liu, T., Xiao, L., Jiang, X., Zheng, X., 2012. High-efficiency removal of NOx using a combined adsorption-discharge plasma catalytic process. Environ. Sci. Technol. 46 (4), 2337–2344.
Zhang, G., Wang, T., Zhou, J., Guo, H., Qu, G., Guo, X., Jia, H., Zhu, L., 2022. Intrinsic mechanisms underlying the highly efficient removal of bacterial endotoxin and related risks in tailwater by dielectric barrier discharge plasma. Water Res. 226, 119214.
Zhang, H., Li, P., Zhang, A., Sun, Z., Liu, J., Héroux, P., Liu, Y., 2021. Enhancing interface reactions by introducing microbubbles into a plasma treatment process for efficient decomposition of PFOA. Environ. Sci. Technol. 55 (23), 16067–16077.
Zhang, Z., Li, B., Li, N., Sardar, M.F., Song, T., Zhu, C., Lv, X., Li, H., 2019. Effects of UV disinfection on phenotypes and genotypes of antibiotic-resistant bacteria in secondary effluent from a municipal wastewater treatment plant. Water Res. 157, 546–554.
Zhou, J., Wang, T., Xie, X., 2020. Locally Enhanced Electric Field Treatment (LEEFT) promotes the performance of ozonation for bacteria inactivation by disrupting the cell membrane. Environ. Sci. Technol. 54 (21), 14017–14025.
Zhu, Y., Shcherbanev, S., Baron, B., Starikovskaia, S., 2017. Nanosecond surface dielectric barrier discharge in atmospheric pressure air: I. measurements and 2D modeling of morphology, propagation and hydrodynamic perturbations. Plasma Sources Sci. Technol. 26 (12), 125004.
Zhu, Z.Z., Zhang, M.Y., Wang, L.G., Zhang, J.Y., Luo, S.T., Wang, Z.F., Guo, L., Liu, Z.J., Liu, D.X., Rong, M.Z., 2023. Comparison of discharge mode transition of air plasma under pulsed and sinusoidal excitations. J. Phys. D-Appl. Phys. 56 (35).